

Performance evaluation of procedures used to correct measured *I-V* characteristics of photovoltaic modules for temperature and irradiance

Wenhai Xu¹ | Christos Monokroussos¹  | Harald Müllejans² | Werner Herrmann³

¹TÜV Rheinland (Shanghai) Co., Ltd., Shanghai, China

²Joint Research Centre (JRC), European Commission, Ispra, Italy

³TÜV Rheinland Solar GmbH, Cologne, Germany

Correspondence

Christos Monokroussos, TÜV Rheinland (Shanghai) Co., Ltd., Shanghai, China.
 Email: christos.monokroussos@tuv.com

Abstract

IEC 60891 ed.3 published in 2021 has defined four standard *I-V* characteristics correction procedures numbered 1 through 4. The aim of this work is to evaluate these four *I-V* translation methods. The results show that correction procedure 1 (CP1) and 2 (CP2) work well over a broad range of irradiances and temperatures. However, CP1 requires *I-V* curves being measured adequately down to negative current regime at low-irradiance levels and CP2 is not so suitable for low shunt-resistance modules; both also require a set of correction parameters. Based on our performance analysis, a new method based on CP2 is introduced to improve the correction performance for low shunt-resistance modules; the mean bias error (MBE) value of maximum power (P_{MAX}) improved from -10.26% to -1.32% . Correction procedure 3 (CP3) employs a drastically different correction procedure as compared with the other CPs. This work shows that CP3 works well over a broad range of irradiances and temperatures, but significant distortion of the corrected *I-V* curves may occur when extrapolation is required. Correction procedure 4 (CP4) requires only a single *I-V* curve and shows generally good results in short-circuit current (I_{SC}) but worse agreement in open-circuit voltage (V_{OC}) and P_{MAX} .

KEY WORDS

characterization, *I-V* curve translation, PV module, PV testing

1 | INTRODUCTION

Photovoltaic (PV) technology is regarded as one of the promising approaches to solve the global energy crisis. In the last two decades, the global PV market grew rapidly. The energy yield of PV modules is an important parameter to evaluate them, and it can be predicted based on their electrical performance. The electrical performance of PV modules is assessed by measuring their current–voltage characteristics (*I-V* curves), which contain information such as short-circuit current, I_{SC} , open-circuit voltage, V_{OC} , and maximum power, P_{MAX} .

The views expressed are purely those of the authors and may not in any circumstances be regarded as stating an official position of the European Commission.

Following standards of the International Electrotechnical Commission (IEC), these electrical parameters of PV modules in general have to be reported and specified at standard test conditions (STC), which are defined as 1000W/m^2 of irradiance, 25°C of device temperature and the reference solar spectrum tabulated in IEC 60904-3 (AM1.5).^{1,2} However, the actual measurement conditions will usually deviate from STC. Therefore, methods for *I-V* curve correction are necessary to translate the measured *I-V* curves to STC. Furthermore, the same methods allow to predict the performance of PV modules at irradiance and temperature conditions encountered in the field, based on laboratory measurements under an irradiance-temperature matrix. The matrix includes various representative irradiance-temperature conditions, which could occur under real conditions.

The international standard IEC 60891:2021³ includes four different procedures to correct *I-V* curves for temperature and irradiance deviations from the reporting conditions. Correction procedure 1 (CP1) has been included already since the first edition of IEC 60891 in 1987. It is based on the work published by J.D. Sandstorm,⁴ and it utilizes the simplified single-diode model to describe the PV junction. In 2009, correction procedure 2 (CP2) and correction procedure 3 (CP3) were introduced in the second edition of IEC 60891. CP2 is still based on the simplified single-diode model, with six parameters for the *I-V* curve correction, and it was initially proposed by W. Herrmann and co-workers.⁵ CP3 utilizes multiple *I-V* curves to perform a linear interpolation or extrapolation for correction. This method requires no fitting parameters and was proposed by Y. Hishikawa and co-workers.⁶ Finally, correction procedure 4 (CP4) was introduced in the third edition of IEC 60891 in 2021, and it is based on the work by Y. Hishikawa and co-workers.⁷ CP4 is based on a simplified single-diode model from a single *I-V* curve, similarly to CP1 and CP2. Therefore, it is suitable in cases where further information is not known and cannot be extracted.⁷

The goal of the work discussed in this paper is to use six different modules, with *I-V* curves measured (or simulated) under all reporting test conditions, to evaluate the performance of these four *I-V* translation procedures included in IEC 60891:2021. This work also explores the applicability of each correction method under different irradiance and temperature conditions. The work demonstrates that all four CPs perform accurate correction over a broad range of irradiances and temperatures, but each method has its own limitations and disadvantages. The user should be aware of the advantages and disadvantages of each method in order to apply the most appropriate CP to the available set of data.

2 | METHODOLOGY

2.1 | Test samples

As shown in Table 1, the test samples consist of three types of high efficiency (HE) c-Si modules (one type of p-type PERC and

two types of n-type HJT). Three types of synthetic *I-V* curves (one for a low shunt-resistance module, one for a high series-resistance module and one for a defect-free module) were calculated for the evaluation of the CPs. Device under test (DUT) HJT-2 was measured with a negative current regime that was limited to -1 A , which is the least negative value between the six cases; its *I-V* curve was specifically selected, which was measured with a small value of negative current, to investigate the effect of the latter on the *I-V* curve translation. As shown in Figure 1, the negative current regime is the *I-V* curve where the current is negative under forward voltage.

2.2 | Simulations and measurements

Synthetic *I-V* curves were modelled by Herrmann's one-diode model, modified from Bishop's model.^{8,9} These *I-V* curves were generated by applying the following equations:

$$I = I_{ph} - I_0 \times \left[\exp\left(\frac{V + IR_s}{\eta N_s V_T}\right) - 1 \right] - \frac{V + IR_s}{R_{sh}} \quad (1)$$

$$V_T = \frac{kT}{q} \quad (2)$$

$$I_{ph} = \frac{G}{1000} \times \{I_{ph,STC} \times [1 + \alpha_{rel} \times (T - 25)]\} \quad (3)$$

$$I_0 = I_{0,STC} \times \exp\left(-\frac{E_g}{kT}\right) \quad (4)$$

$$E_g = E_{g0} - \frac{c_1 \times T^2}{c_2 + T} \quad (5)$$

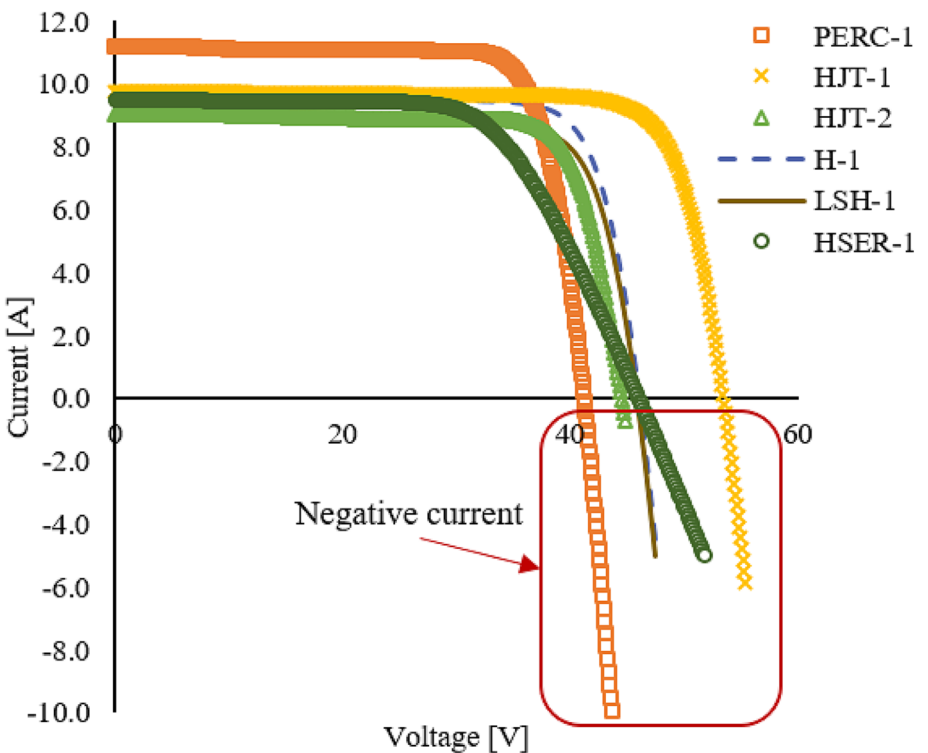
where

- E_g is energy band gap of silicon that can be calculated from Equation (5);
- $E_{g0} = 1.17\text{ eV}$, E_{g0} is the energy band gap of silicon at 0 K;

TABLE 1 Test modules type and corresponding identification. The related short-circuit current, open-circuit voltage, maximum power, all measured at STC, and the negative current regime are shown in the table.

Identification	Module type	Short-circuit current (I_{sc})	Open-circuit voltage (V_{oc})	Maximum power (P_{MAX})	Negative current regime
Measured modules					
PERC-1	p-type PERC	11.20 A	41.21 V	366.97 W	Up to -10 A
HJT-1	n-type HJT	9.77 A	53.44 V	417.76 W	Up to -6 A
HJT-2	n-type HJT	9.02 A	44.51 V	320.62 W	Up to -1 A
Simulated modules					
H-1	Defect-free module	9.50 A	45.99 V	350.51 W	Up to -5 A
LSH-1	Low shunt-resistance	9.47 A	45.82 V	322.82 W	Up to -5 A
HSER-1	High series-resistance	9.48 A	45.99 V	283.37 W	Up to -5 A

FIGURE 1 The I-V curves of the six DUTs at STC. The area enclosed by the red line defines the negative current regime.



- c_1 and c_2 are the silicon material constants which equal to 4.73×10^4 eV/K and 636 K respectively;
- I and V are the current and voltage of the DUT, respectively;
- T is the temperature of the module;
- V_T is the thermal voltage;
- k is the Boltzmann constant (1.381×10^{-23} J/K);
- q is the elementary charge (1.602×10^{-19} C);
- I_{ph} is the photogenerated current;
- $I_{ph,STC}$ is the photogenerated current under STC;
- I_0 is the saturation current;
- $I_{0,STC}$ is the saturation current under STC;
- R_{sh} is the shunt resistance;
- R_s is the series resistance;
- α_{rel} is the relative temperature coefficient of the short-circuit current;
- η is the cell ideality factor;
- N_S is the number of cells in a module.

The values of the simulation parameters used in this work are presented in Table 2.

The I-V measurements were acquired in the laboratory of TÜV Rheinland in Shanghai, as part of the ordinary testing of PV modules. We employed a Dynamic I-V sweep method¹⁰ with a pulsed solar simulator (>80 ms) to characterize the DUTs electrically. A World Photovoltaic Scale (WPVS) reference cell calibrated at Physikalisch-Technische Bundesanstalt (PTB) was used as a reference cell.

All DUTs were simulated or measured at seven different levels of irradiance (100, 200, 400, 600, 800, 1000 and 1100 W/m²) and four

TABLE 2 The input parameters of simulated solar modules. Low R_{sh} and high R_s were used in the low shunt-resistance and high series-resistance condition, respectively.

Parameter	Value
$I_{ph,STC}$ (A)	9.5
$I_{0,STC}$ (A)	1.5^{-10}
Ordinary R_s (Ω)	0.15
High R_s (Ω)	1
Ordinary R_{sh} (Ω)	600
Low R_{sh} (Ω)	50
η	1
α_{rel} (%/K)	0.05
N_S	72
E_{g0} (eV)	1.17

different temperatures (15°C, 25°C, 50°C, 75°C). The selection of irradiances and temperatures corresponds to the whole range of the irradiance-temperature matrix in IEC 61853-1,¹¹ which results in 22 different reporting test conditions including STC (see Section 2.4 and Figure 4).

2.3 | Review of correction procedures

The four translation methods applied in this work are described in IEC 60891:2021.³ The equations of these methods are provided below for the reader's convenience.

2.3.1 | CP1

The equations used in CP1 are as follows:

$$I_2 = I_1 + I_{SC1} \times \left(\frac{G_2}{G_1} - 1 \right) + \alpha \times (T_2 - T_1) \quad (6)$$

$$V_2 = V_1 - R_S \times (I_2 - I_1) - \kappa \times I_2 \times (T_2 - T_1) + \beta \times (T_2 - T_1) \quad (7)$$

where

- I_1 , V_1 , T_1 and G_1 are the measured current, voltage, module temperature and irradiance, respectively;
- I_2 and V_2 are the corresponding pair of current and voltage values of the corrected I - V curve;
- T_2 and G_2 are the target module temperature and irradiance respectively;
- I_{SC1} is the measured short-circuit current;
- R_S is the internal series resistance;
- α and β are respectively the short-circuit current and open-circuit voltage temperature coefficients at the target irradiance for correction;
- κ is the curve correction factor.

The determination of the four correction parameters, α , β , R_S and κ will be mentioned in Section 2.3.6.

2.3.2 | CP2

The equations used in CP2 are as follows:

$$I_2 = \frac{G_2}{G_1} \times I_1 \times \frac{(1 + \alpha_{rel} \times (T_2 - 25))}{(1 + \alpha_{rel} \times (T_1 - 25))} \quad (8)$$

$$V_2 = V_1 - R'_{S1} \times (I_2 - I_1) - \kappa' \times I_2 \times (T_2 - T_1) + V_{OC,STC} \times \left\{ \beta_{rel} \times [f(G_2) \times (T_2 - 25) - f(G_1) \times (T_1 - 25)] + \frac{1}{f(G_2)} - \frac{1}{f(G_1)} \right\} \quad (9)$$

$$R'_{S1} = R'_S + \kappa' \times (T_1 - 25) \quad (10)$$

$$V_{OC,STC} = \frac{V_{OC1} \times f(G_1)}{1 + \beta_{rel} \times (T_1 - 25) \times f^2(G_1)} \quad (11)$$

$$f(G) = \frac{V_{OC,STC}}{V_{OC}(G)} = B_2 \times \ln^2 \left(\frac{1000}{G} \right) + B_1 \times \ln \left(\frac{1000}{G} \right) + 1 \quad (12)$$

where

- $V_{OC,STC}$ is the open-circuit voltage at STC. It can be calculated from Equation (11);
- β_{rel} is the relative open-circuit voltage temperature coefficient;
- R'_S is the internal series resistance determined at 25°C,

- R'_{S1} is the internal series resistance at measured temperature T_1 ; it can be calculated from Equation (10);
- κ' is the temperature coefficient of the internal series resistance R'_S ;
- B_1 is the irradiance linear correction factor for V_{OC} that is related to the diode thermal voltage of the p-n junction and the number of cells N_S serially connected in the DUT;
- B_2 is the irradiance correction factor for V_{OC} , which accounts for nonlinearity of V_{OC} with irradiance.

The determination of the six correction parameters α_{rel} , β_{rel} , R'_S , κ' , B_1 and B_2 is described in Section 2.3.6.

2.3.3 | Low-shunt CP2

In this work, a new translation method is developed based on CP2, named, low-shunt CP2. The procedure aims at improving the performance of CP2 on low shunt-resistance modules by extracting the straight-line slope of the I - V curve near I_{SC} from the measured and translated I - V curves. The benefit of the method is that it can still yield complete I - V curves near I_{SC} even for the case of low shunt-resistance PV devices. The low-shunt CP2 workflow is shown in Figure 2.

The additional equations to calculate the translated I - V curve are as follows:

$$I'_2 = I_2 + (m_{meas} - m_{target}) \times V_1 \quad (13)$$

$$V'_2 = V_1 - R'_{S1} \times (I'_2 - I_1) - \kappa' \times I'_2 \times (T_2 - T_1) + V_{OC,STC} \times \left\{ \beta_{rel} \times [f(G_2) \times (T_2 - 25) - f(G_1) \times (T_1 - 25)] + \frac{1}{f(G_2)} - \frac{1}{f(G_1)} \right\} \quad (14)$$

where

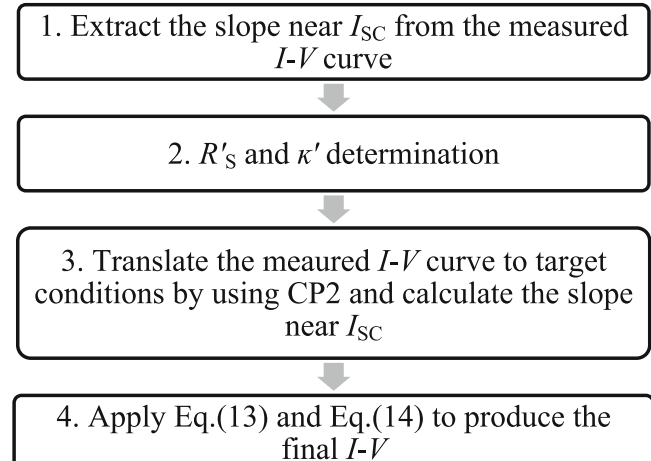


FIGURE 2 The workflow of low-shunt CP2.

- V'_2 and I'_2 are the coordinates of the corresponding points on the final corrected I - V curve;
- m_{meas} and m_{target} are the slopes of the I - V curve near I_{SC} calculated in step 1 and step 3, respectively;

All the other parameters used in step 3 are kept as in CP2. Please note that for step 4, I_2 from step 3 is required, but not V_2 . Essentially, in step 4 first I'_2 is calculated, based on I_2 and V_1 (Equation 13). Then V'_2 is calculated based on I'_2 , I_1 and V_1 . The determination of R 's and κ' will be mentioned in Section 2.3.6.

2.3.4 | CP3

The equations at the core of CP3 are as follows:

$$V_3 = V_1 + \gamma \times (V_2 - V_1) \quad (15)$$

$$I_3 = I_1 + \gamma \times (I_2 - I_1) \quad (16)$$

which are based on two measured I - V curves 1 and 2. V_3 and I_3 are the corresponding pair of voltage and current on the corrected I - V curve at the target irradiance G_3 and target temperature T_3 ; γ is an interpolation constant that is related to the irradiance and temperature according to the following equations:

$$G_3 = G_1 + \gamma \times (G_2 - G_1) \quad (17)$$

$$T_3 = T_1 + \gamma \times (T_2 - T_1) \quad (18)$$

The points (I_1, V_1) on the first curve and (I_2, V_2) on the second curve should be chosen so that

$$I_2 - I_1 = I_{\text{SC}2} - I_{\text{SC}1} \quad (19)$$

CP3 requires no correction parameters, contrary to CP1, CP2 and CP4. However, CP3 requires DUTs have good linearity for interpolation and extrapolation. In practice, only few data points on the I - V curve 2 exactly satisfy Equation (19); therefore, V_2 and I_2 are required to be calculated from an interpolation of I - V curve 2. Based on Equations (17) and (18), the target temperature and the target irradiance are not independent. CP3 requires two measured I - V curves to obtain one I - V curve corrected or translated at a specified irradiance or temperature. The user is allowed to set the target irradiance alone or the target temperature alone; the other parameter (i.e., temperature or irradiance, respectively) will be determined consequently. CP3 requires two I - V curves measured at the target irradiance or at the target temperature to obtain a final corrected I - V curve with both desired target irradiance and temperature. To obtain this objective, CP3 requires linear interpolation or linear extrapolation of at least three measured I - V curves (see Section 2.4.2). Furthermore, CP3 can also be used with more than three (viz., four) measured I - V curves. The three-curve CP3 (3C-CP3)

and four-curve CP3 (4C-CP3) method is detailed in Section 2.4.2 and Figures 5 and 6.

2.3.5 | CP4

The equations used in CP4 are as follows:

$$I'_1 = I_1 + I_{\text{SC}1} \times \left(\frac{G_2}{G_1} - 1 \right) \quad (20)$$

$$V'_1 = V_1 - R_S \times (I'_1 - I_1) \quad (21)$$

$$I_2 = I'_1 + \alpha_{\text{rel}} \times I_{\text{SC,STC}} \times (T_2 - T_1) \quad (22)$$

$$V_2 = V'_1 + (T_2 - T_1) \times \frac{1}{T_1} \times (V'_1 - N_S \times \varepsilon) \quad (23)$$

where

- I_1 and V_1 are coordinates of points on the measured I - V curve;
- I_2 and V_2 are coordinates of corresponding points on the I - V curve corrected for irradiance and temperature;
- I'_1 and V'_1 are the corrected current and voltage for a specified irradiance;
- G_1 is the measured irradiance;
- G_2 is the target irradiance for the DUT;
- $I_{\text{SC,STC}}$ is the short-circuit of the DUT at STC;
- ε is a device-dependent constant with a recommended value of 1.232 V for c-Si PV devices. It can also be calculated with the following equation:

$$\varepsilon = \frac{\eta E_g}{q} \quad (24)$$

- q is the elementary charge (1.602×10^{-19} C);
- η is the diode ideality factor;
- E_g is the bandgap of the DUT material.

In this work, ε is set to 1.232 V for all cases, as suggested in IEC 60891:2021. The use in CP4 of the R_S as determined by the same procedure as used in CP1 for CP4 is defined as CP4*. The determination of R_S of CP4 would be mentioned in Section 2.3.6.

2.3.6 | Correction parameters determination

There are several correction parameters needed to be determined prior to I - V curves translation, namely, α , β , R_S and κ in CP1; α_{rel} , β_{rel} , R 's, κ' , B_1 and B_2 in CP2 and low-shunt CP2; α_{rel} and R_S in CP4 and CP4*. All the correction parameters are listed in the supporting

information Table S43. The determination method of these correction parameters are described in IEC 60891:2021.

The determination of the temperature coefficients α , α_{rel} and β , β_{rel} for all CPs requires multiple *I-V* curves measured at various temperatures, but at constant irradiance, as described in IEC 60891:2021 clause 5. The determination of κ and κ' also requires multiple measured *I-V* curves of the DUT at constant irradiance, but at different temperatures, as described in IEC 60891:2021 clause 7.

The determination of R_S and R'_S requires multiple *I-V* curves measured at different irradiance levels covering the range of interest and at a constant temperature, as described in IEC 60891:2021 clause 6. These *I-V* curves are required to translate to the highest irradiance of interest with $R_S = 0 \Omega$ (or $R'_S = 0 \Omega$) as starting value. To determine the proper R_S in CP1 (or R'_S in CP2), it is required to increase R_S (or R'_S) until the translated *I-V* curves overlap in the range from the voltage at maximum power point (V_{MPP}) to V_{OC} . It is to be noted that low-shunt CP2 utilizes the same determination process to obtain R'_S . Seven curves measured at 25°C with different irradiance (100, 200, 400, 600, 800, 1000 and 1100 W/m²) are used to calculate R_S (or R'_S). The determination of B_1 and B_2 uses a similar method with $R'_S = 0 \Omega$, $B_1 = 0$ and $B_2 = 0$ as starting values, which is also described in clause 6.

R_S in CP4 can be determined from a single *I-V* curve according to the method presented in the clause 6.5 in IEC 60891:2021, which is proposed in the publication by Hishikawa et al.⁷ The method requires to plot a straight line, Y versus X, which is described by the equations:

$$Y = -\frac{V_a - V_b}{I_a - I_b} \quad (25)$$

$$X = -\{\ln(I_{sc} - I_a) - \ln(I_{sc} - I_b)\}/(I_a - I_b) \quad (26)$$

(V_a , I_a) and (V_b , I_b) are two data points on the same *I-V* curve. The y-intercept of the straight line is R_S . IEC 60891 requires a minimum of 10 pairs of data points, a constraint on the coefficient of determination (R^2), which has to be larger than 0.995, and a constraint on the X range to consider, which has to be larger than twice the X minimum value considered.³ The requirements of the method are difficult to satisfy for all the *I-V* curves. R_S for CP4 is therefore determined by utilizing a reference STC curve measured at target condition (see Section 2.4) and alternatively by the same procedure as used in CP1, which is allowed in IEC 60891.³

2.4 | Methodology

In summary, CP1, CP2 and CP4 require one measured *I-V* curve with several correction parameters to obtain the corrected *I-V* curve. On the contrary, CP3 utilizes a linear interpolation or extrapolation approach based on multiple measured *I-V* curves (at least three *I-V* curves), but it requires no correction parameter. Since CP3 is a drastically different correction procedure, the description of the

methodology used for its performance evaluation is provided in a separate Section 2.4.2.

If the *I-V* curves are not measured adequately into the negative current regime, CP1, CP3 and CP4 could result in incomplete *I-V* curves, where the high-voltage regime (V_{MPP} to V_{OC}) is missing. In this case, quadratic regression is used to extract the V_{OC} of the translated *I-V* curves. As shown in Figure 3, the V_{OC} prediction by quadratic regression results in better curve fitting than linear regression, when the high voltage regime is missing. The data points from V_{MPP} to the largest measured voltage were used for regression fitting and then extrapolated to V_{OC} . The linear regression is applied to predict I_{sc} for all methods and for the V_{OC} for CP2, since CP2 inherently always produces complete *I-V* curves.

2.4.1 | Evaluation method for CP1, CP2, low-shunt CP2, CP4 and CP4*

To investigate the performance of CP1, CP2, low-shunt CP2, and CP4 and CP4*, the verification method we used in this work relies on translating 21 curves to STC, and on comparing the new calculated I_{sc} , V_{oc} and P_{MAX} with the corresponding reference curve measured (or simulated) at STC. The 22 points used in this work, as shown in Figure 4, consist in the irradiance and temperature matrix of additional reporting test conditions as detailed in IEC 61853-1.¹¹ The methodology applied in this work, which translates all the measured *I-V* curves to STC is only used for the investigation of the performance of the correction procedures, but in general similar large corrections are not allowed in IEC 60904-1.

To evaluate and validate the procedures in terms of agreement in I_{sc} , V_{oc} and P_{MAX} with their values from the reference *I-V* curve, we

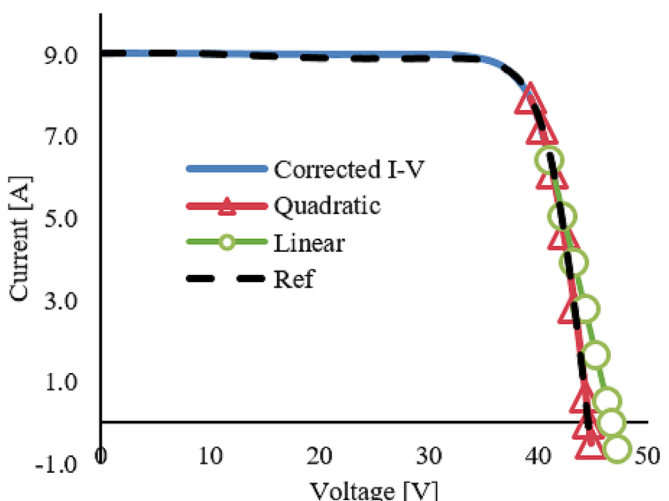
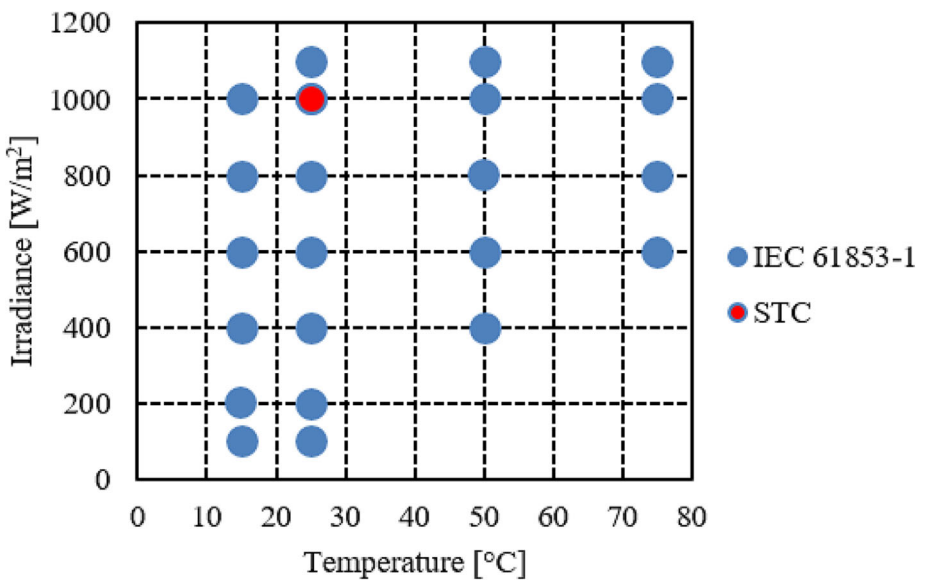


FIGURE 3 The blue *I-V* curve is of HJT-2, measured at 200 W/m² and 25°C, corrected to STC by CP1. The black dashed curve is the reference *I-V* curve measured at STC. The red and green curves present respectively the quadratic and linear extrapolation for V_{OC} prediction from the blue curve, which is missing the high-voltage regime.

FIGURE 4 The irradiance-temperature matrix diagram representing the 22 reporting test conditions used for the power-matrix measurements as per IEC 61853-1. The red dot identifies STC.



have employed the mean bias error (MBE), and the root mean squared error (RMSE), for I_{SC} , V_{OC} and P_{MAX} . MBE is used for estimating the average bias in the I - V curve correction procedures. MBE closer to zero generally indicates better results. The disadvantage of MBE is that the positive and negative errors can cancel out. RMSE is used widely in statistical evaluation, because it indicates the average magnitude of errors. In addition, RMSE is more sensitive to the outliers.¹² In this work, we regard that the MBE and RMSE values of the three electrical parameters within $\pm 1\%$ are acceptable. MBE and RMSE were determined by the following formulae:

$$MBE = \frac{\sum P_{devSTC}}{n} \quad (27)$$

$$RMSE = \sqrt{\frac{\sum^n (P_{devSTC})^2}{n}} \quad (28)$$

$$P_{devSTC} = \frac{X_c - X_{ref}}{X_{ref}} \times 100 \quad (29)$$

where

- P_{devSTC} is the percentage deviation in I_{SC} , V_{OC} and P_{MAX} of the translated I - V curves from the reference curve at STC;
- X_c and X_{ref} represent in turn the three electrical parameters as taken from the corrected and the reference I - V curves, respectively.

2.4.2 | Evaluation method for CP3

In this work, a two-step procedure was applied to three and four I - V curves according to CP3.³ The illustration of the two-step procedure for the three-curve case is shown in Figure 5A (for interpolation) and

(B) (for extrapolation), and the four-curve case is shown in Figure 6A (for interpolation) and (B) (for extrapolation).

As shown in Figure 5, the first step is to utilize two measured (or simulated) I - V curves to generate two intermediate I - V curves translated at the target irradiance, G_m . At the second step, these two intermediate I - V curves are the starting point to obtain the final I - V curve translated at the target temperature, T_m . The two intermediate I - V curves are obtained, respectively, from Curve 1 and Curve 2, and from Curve 2 and Curve 3 in the example we give for the three-curve method. For the four-curve method, the two intermediate I - V curves are calculated, respectively, from Curve 1 and Curve 2, and from Curve 3 and Curve 4.

The I - V curve selection is shown in Table 3. It is noted that a change of order of I - V curves may change the correction results when the device is not linear. The selected I - V curves were translated to the 22 reporting test conditions defined in the IEC 61853-1 irradiance-temperature matrix as shown in Figure 4. The measured (or simulated) I - V curve at each reporting test condition was compared with the translated I - V curves in terms of I_{SC} , V_{OC} and P_{MAX} . Both linear interpolation and extrapolation were employed to build the whole matrix starting from the selected I - V curves. The performance of both 3C-CP3 and 4C-CP3 is presented in Section 3.3. MBE and RMSE are also employed to validate and evaluate both CP3 methods in terms of agreement in three electrical parameters.

3 | RESULTS AND DISCUSSION

Table 4 shows the results of all the methods in terms of MBE and RMSE of I_{SC} , V_{OC} and P_{MAX} for all six DUTs. The deviations of each electrical parameters of each DUT are reported as tables in the supporting information. For all CPs except CP3, the results were obtained by translating 21 I - V curves measured at various reporting test conditions (see Figure 4) to STC and comparing with the corresponding

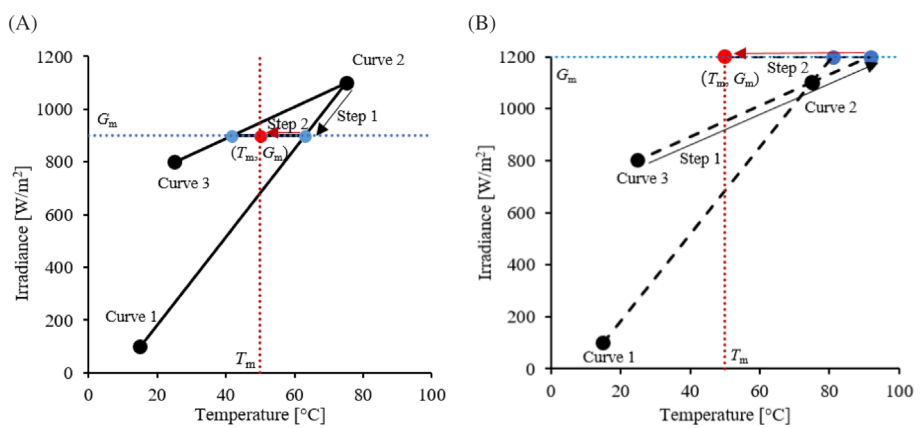


FIGURE 5 (A) The linear interpolation and (B) the linear extrapolation for the two-step procedure of 3C-CP3. Black dots are the measured (or simulated) I-V curves. Blue dots represent the intermediate curves, which are obtained by translation of measured I-V curves to a target common irradiance. The red dot represents the target I-V curve as corrected to the target pair of irradiance and temperature. The solid and dashed lines indicate interpolation and extrapolation, respectively. The black and red arrow represent step 1 and step 2, respectively. The blue and red dashed lines represent the target G_m and target T_m , respectively. The test conditions of the three selected I-V curves are shown in Table 3.

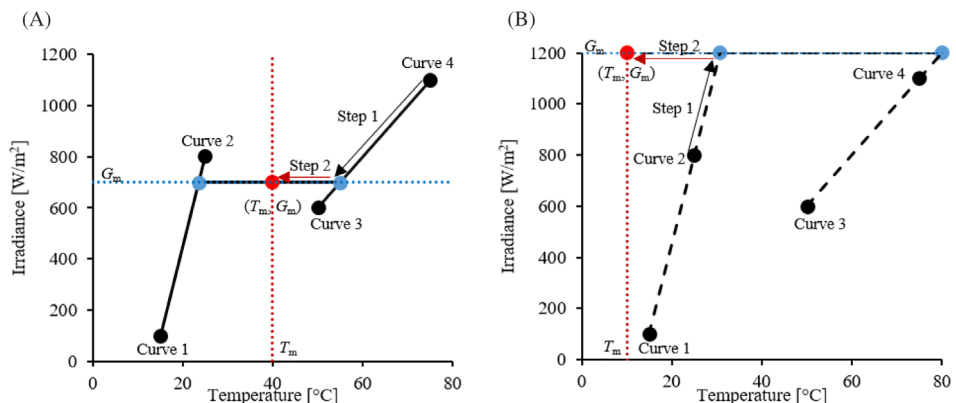


TABLE 3 3C-CP3 and 4C-CP3 I-V curve selection as shown in Figures 5 and 6, respectively.

I-V curve	Reporting test condition
3C-CP3	
Curve 1	100 W/m ² , 15°C
Curve 2	1100 W/m ² , 75°C
Curve 3	800 W/m ² , 25°C
4C-CP3	
Curve 1	100 W/m ² , 15°C
Curve 2	800 W/m ² , 25°C
Curve 3	600 W/m ² , 50°C
Curve 4	1100 W/m ² , 75°C

STC reference curve in terms of three electrical parameters. For the two CP3 methods, the selected I-V curves were translated to all 22 reporting test conditions, including STC. The results were obtained by the comparison of translated I-V curves and the measured I-V curves at the corresponding reporting test condition.

3.1 | Performance and evaluation of CP1

As shown in Table 4, the MBE values of I_{SC} produced by CP1 are within $\pm 0.28\%$. The MBE of V_{OC} and P_{MAX} are within $\pm 0.23\%$ and $\pm 0.37\%$, respectively. The RMSE of I_{SC} is within $\pm 0.75\%$, and RMSE of V_{OC} is within $\pm 0.67\%$. The RMSE of P_{MAX} is within $\pm 0.73\%$. Generally, CP1 produced consistently accurate corrections for all three electrical parameters, because MBE and RMSE of all three parameters are within $\pm 1\%$. The most relevant exception to this is the case of test module HJT-2, which is the module for which the measured negative current was limited to -1 A (see Table 1). As shown in Table 4, for the DUT HJT-2 a nearly-zero MBE value is observed for V_{OC} , 0.07%, while the corresponding RMSE of V_{OC} for CP1 is 0.67%. The large RMSE value, when compared with the nearly-zero MBE value, indicates that some reporting test conditions may have produced outliers in V_{OC} . Meanwhile, a low value of MBE and RMSE for I_{SC} and P_{MAX} of HJT-2 is observed. The MBE and RMSE of I_{SC} are 0.18% and 0.3%, respectively. The values of P_{MAX} are 0.02% and 0.43%, respectively. A high deviation in V_{OC} is observed at low-irradiance levels as shown in Figure 7B and in Table S15 in the

TABLE 4 MBE and RMSE of I_{SC} , V_{OC} and P_{MAX} produced by CP1, CP2, low-shunt CP2, 3C-CP3, 4C-CP3, CP4 and CP4*.

MBE		PERC-1	HJT-1	HJT-2	H-1	LSH-1	HSER-1
I_{SC}	CP1	0.05%	0.28%	0.18%	0.02%	0.27%	-0.02%
	CP2	0.04%	0.33%	0.17%	0.14%	2.20%	-0.09%
	Low-shunt CP2	0.02%	0.29%	0.16%	0.04%	0.46%	0.00%
	3-curve CP3	0.62%	0.33%	0.70%	0.77%	0.77%	0.77%
	4-curve CP3	-0.70%	-0.29%	-0.69%	-0.87%	-0.87%	-0.87%
	CP4	0.13%	0.25%	0.20%	0.06%	0.72%	0.01%
	CP4*	0.12%	0.25%	0.20%	0.05%	0.66%	0.01%
V_{OC}	CP1	-0.23%	-0.21%	0.07%	-0.02%	0.06%	-0.04%
	CP2	-0.02%	-0.01%	-0.04%	-0.01%	-0.17%	-0.01%
	Low-shunt CP2	0.01%	0.02%	-0.03%	0.04%	0.61%	0.04%
	3-curve CP3	-0.08%	0.13%	0.80%	0.10%	0.15%	-0.07%
	4-curve CP3	0.06%	0.07%	1.18%	0.10%	-0.01%	-0.16%
	CP4	0.04%	0.33%	0.51%	0.20%	0.81%	0.05%
	CP4*	-0.22%	-0.43%	-0.14%	0.15%	0.24%	0.05%
P_{MAX}	CP1	0.10%	0.37%	0.02%	-0.01%	-0.01%	0.00%
	CP2	-0.03%	0.22%	0.13%	0.09%	-10.26%	0.17%
	Low-shunt CP2	-0.01%	0.44%	0.03%	-0.09%	-1.32%	-0.09%
	3-curve CP3	2.42%	13.07%	1.03%	0.83%	1.07%	0.76%
	4-curve CP3	4.99%	2.39%	0.10%	-0.95%	-1.43%	-0.91%
	CP4	0.45%	1.20%	1.01%	0.38%	1.39%	1.03%
	CP4*	0.14%	0.30%	0.24%	0.31%	0.71%	1.02%
RMSE		PERC-1	HJT-1	HJT-2	H-1	LSH-1	HSER-1
I_{SC}	CP1	0.21%	0.56%	0.30%	0.07%	0.75%	0.10%
	CP2	0.29%	0.67%	0.31%	0.23%	4.30%	0.26%
	Low-shunt CP2	0.25%	0.60%	0.30%	0.07%	0.80%	0.08%
	3-curve CP3	1.33%	1.72%	1.30%	1.62%	1.62%	1.62%
	4-curve CP3	2.52%	1.45%	2.61%	3.04%	2.75%	2.75%
	CP4	0.36%	0.66%	0.40%	0.13%	1.56%	0.15%
	CP4*	0.36%	0.66%	0.40%	0.13%	1.56%	0.15%
V_{OC}	CP1	0.32%	0.34%	0.67%	0.06%	0.15%	0.08%
	CP2	0.04%	0.10%	0.14%	0.02%	0.45%	0.02%
	Low-shunt CP2	0.05%	0.11%	0.14%	0.09%	1.78%	0.09%
	3-curve CP3	0.20%	0.39%	2.10%	0.18%	0.30%	0.19%
	4-curve CP3	0.12%	0.20%	1.42%	0.23%	0.65%	0.26%
	CP4	0.12%	1.05%	1.52%	0.32%	1.02%	0.13%
	CP4*	0.32%	0.70%	0.98%	0.30%	0.36%	0.13%
P_{MAX}	CP1	0.20%	0.73%	0.43%	0.01%	0.01%	0.01%
	CP2	0.30%	0.50%	0.44%	0.95%	19.52%	0.74%
	Low-shunt CP2	0.34%	0.70%	0.42%	0.37%	1.77%	0.39%
	3-curve CP3	5.08%	37.84%	2.29%	1.77%	2.58%	1.65%
	4-curve CP3	10.15%	5.65%	5.16%	3.37%	4.99%	2.95%
	CP4	0.58%	1.96%	1.38%	0.69%	1.83%	2.21%
	CP4*	0.24%	0.75%	0.56%	0.68%	1.51%	2.21%

supporting information. Figure 7 shows the deviations produced by CP1 after correction of the I - V curves to STC over the whole matrix of irradiance and temperature for I_{SC} , V_{OC} and P_{MAX} . The deviations

in V_{OC} at low-irradiance levels (100, 200 and 400 W/m²) vary from -1.12% to 1.72%, whereas the deviations at high-irradiance levels (800, 1000 and 1100 W/m²) are within $\pm 0.44\%$. Figure 7 also

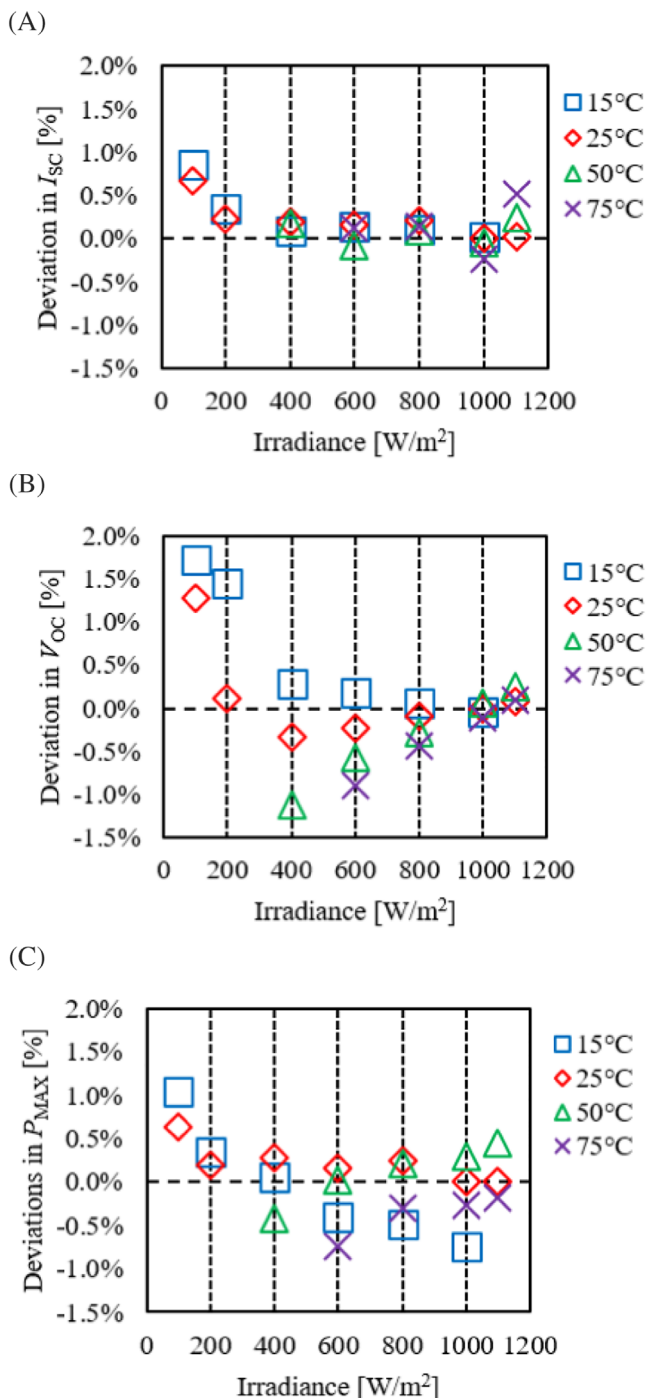


FIGURE 7 The deviation in (A) I_{SC} , (B) V_{OC} and (C) P_{MAX} of the $I-V$ curves translated to STC by utilizing CP1 for HJT-2. The shown DUT exhibited worst-case deviations in V_{OC} for CP1.

indicates a trend according to which the closer a translated curve was measured to the target irradiance, the better correction results were produced in V_{OC} . The variation of correction parameters with temperature/irradiance such as R_S and β could also affect the accuracy of V_{OC} calculation. CP1 introduced κ to correct the variation of R_S with temperature, but the inadequate consideration in CP1 of the

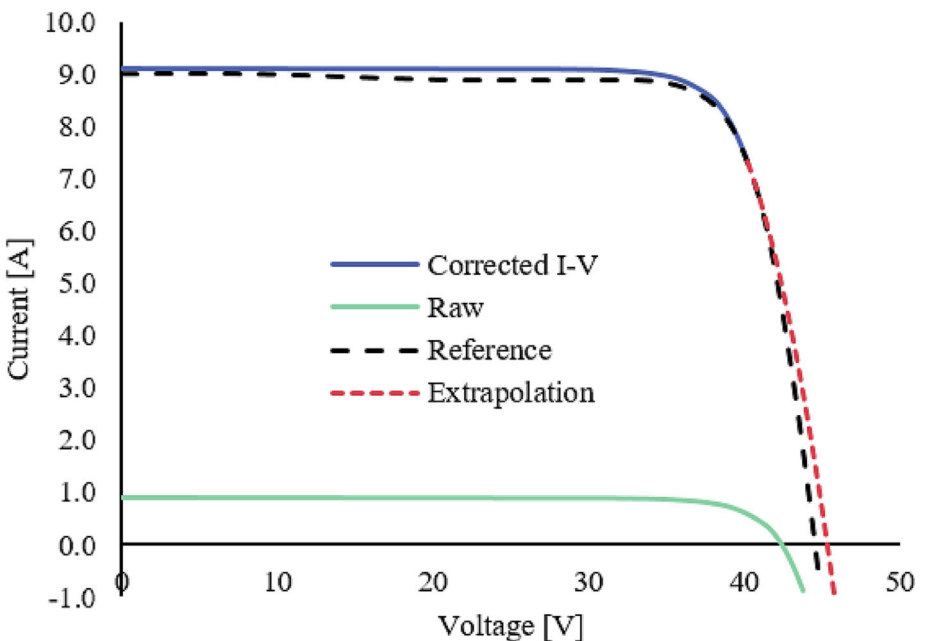
variation in β with irradiance could also affect the calculation of V_{OC} . However, the large deviations in V_{OC} at low-irradiance levels are mainly attributed to the insufficiently-measured negative current regime in the case of HJT-2. As shown in Figure 8, the $I-V$ curve measured at 100 W/m^2 , 15°C is missing the high-voltage regime after correction. This results in an inaccurate V_{OC} with 1.72% deviation by quadratic extrapolation. Consistently to our previous findings these large percentage deviations occurring at low-irradiance levels are mainly due to the $I-V$ curves not being measured adequately far into the negative current regime, so that the high-voltage regime ($\sim V_{OC}$) of the translated $I-V$ curves are missing.

Another drawback of CP1 is also observed in the case of test module LSH-1. As shown in Figure 9A, it seems that the correction of I_{SC} for LSH-1 is strongly associated with the voltage shift caused by temperature near I_{SC} . CP1 produces large deviations ($>1.40\%$) in I_{SC} at 75°C (see Table S29 in the supporting information), whereas the deviations in V_{OC} and P_{MAX} are respectively within $\pm 0.32\%$ and $\pm 0.03\%$. The deviations in I_{SC} are attributed to an inherent property of CP1. In Equation (7), the term $-R_S \times (I_2 - I_1) - \kappa \times I_2 \times (T_2 - T_1) + \beta \times (T_2 - T_1)$ will result in a shift of the whole $I-V$ curve in the voltage-axis. Because low shunt-resistance modules have steep slope in low voltage regime, the shift of an $I-V$ curve on the voltage-axis will significantly affect the intercept with the current-axis, which is the I_{SC} . The modules with high shunt-resistance are not affected, because the slope in the low voltage regime is negligible. It is, therefore, suggested to limit the $I-V$ translation to $\pm 25^\circ\text{C}$ of the target temperature, when the DUT has a low shunt-resistance or significant leakage current.

3.2 | Performance and evaluation of CP2 and low-shunt CP2

In general, CP2 resulted in smaller deviations than CP1 and CP4, regardless of how far the device was measured into the negative current regime. However, it produced significant errors for device (LSH-1) that showed current leakage (low R_{sh}). In Table 4, the RMSE in P_{MAX} of CP2 for LSH-1 is 19.52% . Similarly, the RMSE in I_{SC} and V_{OC} are 4.30% and 0.45% , respectively. As shown in Figure 10, the $I-V$ translation resulted in significant lower accuracy of I_{SC} and P_{MAX} prediction at low-irradiance levels, still showing good agreement for V_{OC} correction. Generally, we observed a trend related to P_{MAX} correction: When the measured irradiance is closer to the target irradiance, the prediction is more accurate. The worst case of P_{MAX} deviation is -56.96% and occurred at 100 W/m^2 , 15°C , where the I_{SC} and V_{OC} deviations are 11.42% and -1.11% , respectively. When the test irradiances are at 1000 and 1100 W/m^2 , the deviations in I_{SC} , V_{OC} and P_{MAX} are within $\pm 1.45\%$, $\pm 0.26\%$ and $\pm 0.68\%$, respectively. The results demonstrate that CP2 is not recommended for translation over irradiances exceeding the general constraints for $I-V$ curve measurements set by IEC 60904-1, that is, $\pm 40\%$ of the target irradiance, when the DUT has low R_{sh} and consequently current leakage. This is attributed to the fact that CP2 significantly distorts the shape of the $I-V$ curve for cases of low R_{sh} , and the corrected $I-V$ characteristics may carry significant

FIGURE 8 The green curve represents the data measured under $100 \text{ W/m}^2, 15^\circ\text{C}$, which is the worst case produced by CP1 of HJT-2. The blue curve is the I - V corrected to STC. The dashed black curve indicates the reference STC I - V curve. The dashed red curve presents the quadratic extrapolation to V_{OC} from the blue curve.



errors as shown in Figures 10 and 11. The distortion of the I - V curve is attributed to the term $\frac{G_2}{G_1}$ in Equation (8). The term $\frac{G_2}{G_1}$ enlarges the negative slope near I_{SC} . This effect is more pronounced for low R_{sh} modules, because low R_{sh} modules always have noticeable negative slopes near I_{SC} while the defect-free modules remain almost flat near I_{SC} . CP2 also resulted in inaccurate P_{MAX} calculations of H-1 at 100 W/m^2 irradiance level test condition (see Table S23) due to the term $\frac{G_2}{G_1}$. In this case, the negative slope near I_{SC} is enlarged by 10 times after translating to STC. To solve these problems, the low-shunt CP2 is developed in this work (see Section 2.3.3 and Figure 12).

As shown in Table 4, the enhancement in the calculated deviations of I_{SC} and P_{MAX} of low-shunt CP2 for LSH-1 is significant. The MBE of P_{MAX} improved from -10.26% to -1.32% and its RMSE decreased from 19.52% to 1.77% . The MBE of I_{SC} decreased from 2.20% to 0.46% and its RMSE decreased, for the same module, from 4.30% to 0.80% . However, both MBE and RMSE of V_{OC} increase, where the MBE is still within $\pm 1\%$, but RMSE is 1.78% . As shown in Figure 12B, the V_{OC} deviations at 100 W/m^2 irradiance are over 5% , and the V_{OC} deviations at 200 W/m^2 irradiance are over 2% , which are significantly larger than the results for CP2. The low-shunt CP2 still needs to improve the performance in V_{OC} at low-irradiance levels. At higher irradiances, the V_{OC} calculated deviations is comparable with CP2 results. The results produced by CP2 and low-shunt CP2 for the other DUTs are mostly comparable to each other, as shown in Table 4. An exception is H-1, for which low-shunt CP2 improved RMSE in P_{MAX} from 0.95% to 0.37% . These improvements are mainly attributed to the enhancements in the translation of 100 W/m^2 irradiance level test condition (see Tables S23 and S24). This suggests that the low-shunt CP2 approach can be universally applied. The disadvantage of the method is that it requires one additional processing step; however, no additional data is required in comparison to CP2.

3.3 | Performance and evaluation of CP3

As stated in Section 2.4.2, the selected I - V curves (Table 3) are translated to all reporting test conditions. The translated I - V curves are compared with the measured (or simulated) I - V curve at each reporting test condition to obtain the results in terms of I_{SC} , V_{OC} and P_{MAX} .

As shown in Table 4, both CP3 methods generate accurate V_{OC} , except for HJT-2. They have significant MBE ($+1.18\%$) and RMSE ($+2.10\%$) for HJT-2 in V_{OC} , while all the MBE and RMSE values in V_{OC} of other five DUTs are within $\pm 0.16\%$ and $\pm 0.65\%$, respectively. The deviations in I_{SC} , V_{OC} and P_{MAX} of HJT-2 produced by 3C-CP3 and 4C-CP3 are shown in Figures 13 and 14, respectively. Figures 13B and 14B indicate a trend according to which higher target irradiance produced higher deviation in V_{OC} . The effect is attributed to the missing part of the I - V curve in the final I - V curve, similarly to the same phenomenon reported for CP1. In the case of HJT-2, the I - V curve measured under $100 \text{ W/m}^2, 15^\circ\text{C}$ (one of the selected curves) is not being measured adequately far enough into the negative current regime. This results in incomplete intermediate I - V curves and the effect propagates to the final I - V curve at the target reporting test condition.

From Table 4, 4C-CP3 shows comparable MBE values with 3C-CP3 in I_{SC} , but the RMSE values are always approximately 1% higher than 3C-CP3, except for HJT-1. The results indicate that 4C-CP3 produces significant outliers in I_{SC} at some specific reporting test conditions. Figures 13A and 14A show the results for the example module HJT-2, for which the 4C-CP3 method generates large deviations (-10.68%) in I_{SC} at $100 \text{ W/m}^2, 25^\circ\text{C}$, while 3C-CP3 produces a deviation of 4.39% . The deviations in I_{SC} from 800 to 1100 W/m^2 produced by 3C-CP3 are within $\pm 1\%$. From 600 to 1100 W/m^2 , 4C-CP3 produces I_{SC} deviations within $\pm 1\%$. 4C-CP3

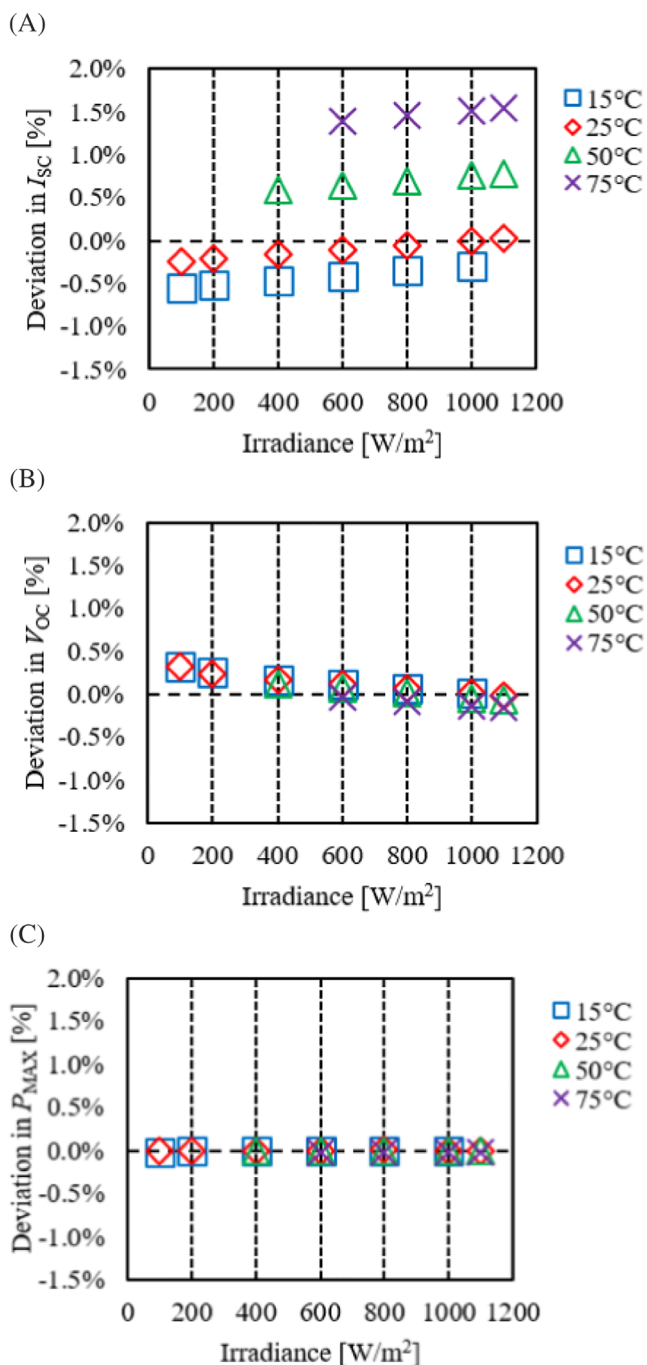


FIGURE 9 The deviation in (A) I_{SC} , (B) V_{OC} and (C) P_{MAX} of the I-V curves translated to STC by utilizing CP1 for LSH-1.

generally produces accurate I_{SC} in a broader irradiance range, but the performance at low-irradiance levels test condition (100 W/m², 25°C) is worse than 3C-CP3. 3C-CP3 also produces inaccurate results at low-irradiance levels test conditions (100 W/m², 25°C), but more accurate than 4C-CP3. This phenomenon appears in all DUTs' results (see supporting information). The problematic result in I_{SC} at the specific reporting test condition is attributed to the linear extrapolation ($\gamma < 0$ or $\gamma > 1$).

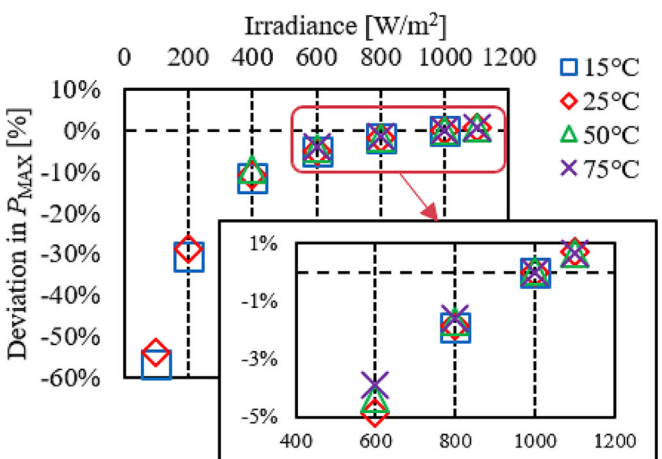


FIGURE 10 The deviation in (A) I_{SC} , (B) V_{OC} and (C) P_{MAX} of translated I-V curves to STC utilizing CP2 for LSH-1. The shown DUT exhibited worst-case deviations in V_{OC} for CP2.

It is noticeable that P_{MAX} has the highest RMSE value among the three electrical parameters for both the 3C-CP3 and the 4C-CP3 method. 4C-CP3 produces higher RMSE values in P_{MAX} than 3C-CP3, except for DUT HJT-1. For HJT-1, 3C-CP3 produces catastrophic results of 13.07% in MBE and 37.84% in RMSE. From our investigation, the low accuracy calculations of P_{MAX} are due to the observable distortions produced in the I-V curve during the extrapolation. The translation without extrapolation always performs accurate calculation (refer to the values identified by the colour blue in the CP3-related tables of the supporting information). When the extrapolation is involved, the translation results are unpredictable.

To explore the relationship between the extrapolation and the observable distortions, two I-V curves from the HJT-2 dataset were chosen to be translated via a single-step CP3 to the reporting test conditions corresponding to different irradiance levels, but at the same temperature of 25°C. As shown in Figure 15A by means of dashed-line style, these two I-V curves are the ones measured, respectively, at 400 W/m², 25°C and 600 W/m², 25°C test conditions. When the I-V curve is extrapolated to lower irradiance, the corrected I-V curve has more serious distortion in the P_{MAX} regime. If the I-V curve is extrapolated to higher irradiances, the translated intermediate I-V curve has more pronounced distortions in the range from I_{SC} to P_{MAX} . The intermediate I-V curve corrected to 1100 W/m² is also missing its part near V_{OC} . Consistently to our previous findings, these large percentage V_{OC} deviations are due to the test module HJT-2 not being measured adequately far enough into the negative current regime.

Other two I-V curves were chosen to be translated to different temperatures, but at the same irradiance level of 600 W/m². The latter are shown in Figure 15B as dashed-line curves. These two I-V curves are measured at 600 W/m², 25°C and 600 W/m², 50°C. If the I-V curve is extrapolated to higher temperature than the target

FIGURE 11 The blue curve represents the data measured under 200 W/m^2 , 25°C , of LSH-1. The red curve is the I-V curve after correction to STC by CP2. The green curve is the I-V curve corrected by low-shunt CP2. The black curve indicates the measured reference STC I-V curve.

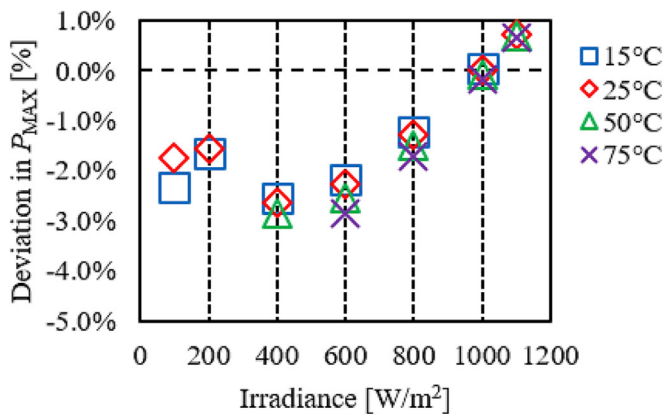
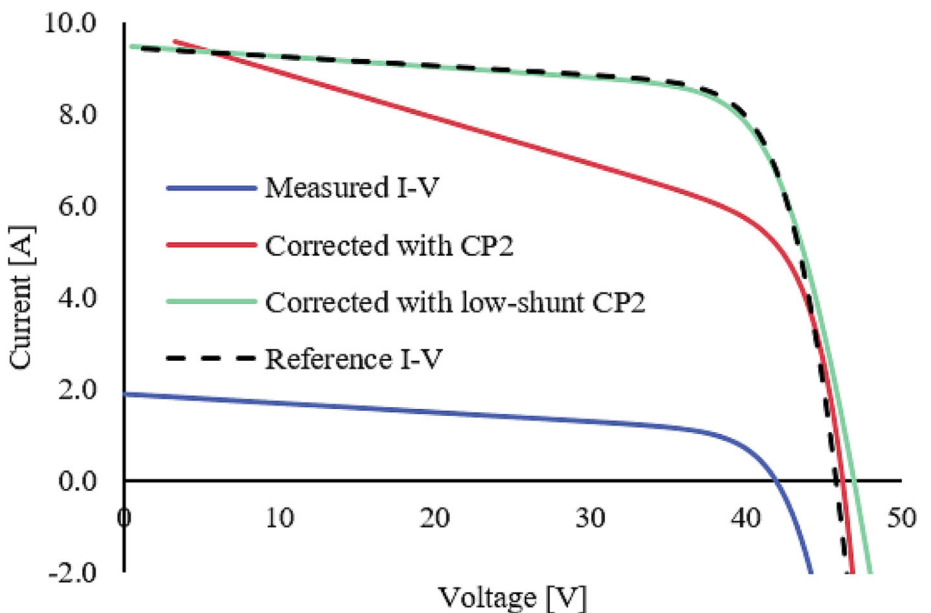


FIGURE 12 The deviation in (A) I_{SC} , (B) V_{OC} and (C) P_{MAX} of translated I-V curves to STC utilizing low-shunt CP2 for test sample LSH-1. Compare with Figure 10, but note differences in vertical scales.

temperature, the distortion will occur around P_{MAX} . If the I-V curve is extrapolated to a lower temperature, it will distort the curve near I_{SC} . From the insets of Figure 15A,B, it seems that a negative γ value could cause a distortion mainly around the P_{MAX} . If γ is larger than 1, the distortion would influence the I-V curve translation from I_{SC} to P_{MAX} . Since both CP3 methods are carried out in two steps, either of which can be represented by the one-step example shown in Figure 15, the distortion could simultaneously affect P_{MAX} and I_{SC} inside one overall correction by either 3C-CP3 or 4C-CP3. In two-step 3C-CP3/4C-CP3, up to three times extrapolation process could be involved. The extrapolation applied on the distorted intermediate I-V curve could result in unpredictable distortion for the final target I-V curve. It is therefore recommended to use the extrapolation with caution. If the extrapolation is inevitable, it is suggested that γ should be as small as possible.

3.4 | Performance and evaluation of CP4 and CP4*

CP4 produced MBE and RMSE comparable to CP1 and CP2 in I_{SC} , V_{OC} for almost all DUTs and test conditions, except HJT-2 and LSH-1 (see Table 4). As discussed in Section 3.2, CP2 produces an erroneous translation for LSH-1 due to its low-shunt resistance, while CP4 produces 1.56% in RMSE for I_{SC} . CP4 produces MBE and RMSE values for V_{OC} of more than 0.5% and 1.5% for HJT-2. The MBE and RMSE in P_{MAX} are over 1% for most DUTs, except PERC-1 and H-1. These large deviations are justifiable by the fact that CP4 is the simplest method to use and requires minimum input parameters.

The HJT-2 results produced by CP4 for the three electrical parameters are shown in Figure 16. As shown in Figure 16, the deviations for CP4 in V_{OC} vary from -1.08% to 3.89% and the deviations in P_{MAX} vary from -0.98% to 3.04% , while the range of deviations for I_{SC} is from -0.52% to 1.10% for DUT HJT-2. Similarly to CP1, high deviations in V_{OC} at low-irradiance levels (100 to 400 W/m^2) were observed for HJT-2 because the I-V curves were not measured sufficiently deep into the reverse current regime, resulting in incomplete I-V curves after translation to STC. A trend is also observed according to which higher measured irradiance results in lower deviations in P_{MAX} at constant temperature in Figure 16C. The low accuracy of P_{MAX} calculation could be attributed to the inaccurate R_S determination.

To validate the accuracy of CP4, the same value of R_S used in CP1 was applied, which is noted in this work as CP4*. As shown in Figure 17C, CP4* calculates P_{MAX} more accurately, with deviations varying from -0.98% to 0.87% . Furthermore, the improvement of the error in I_{SC} is negligible, while calculated deviations also improved for V_{OC} . The worst-case deviation in V_{OC} decreased from 3.89% to 2.05% . From Table 4 CP4* has a significant improvement in P_{MAX} for most DUTs. H-1 and HSER-1 obtain similar results with CP4. The reason is that the R_S value calculated in CP4 is an approximation of the

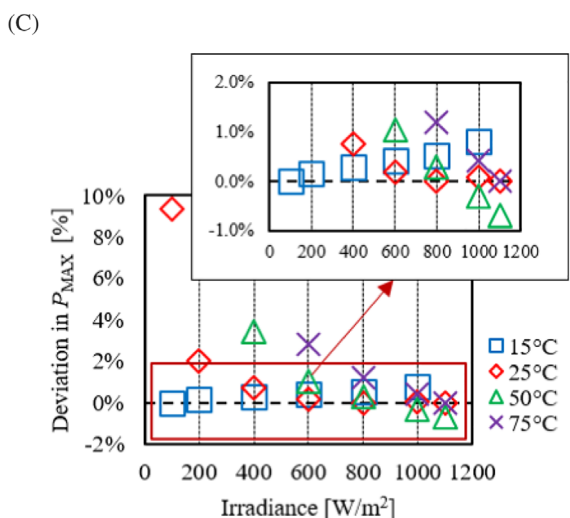
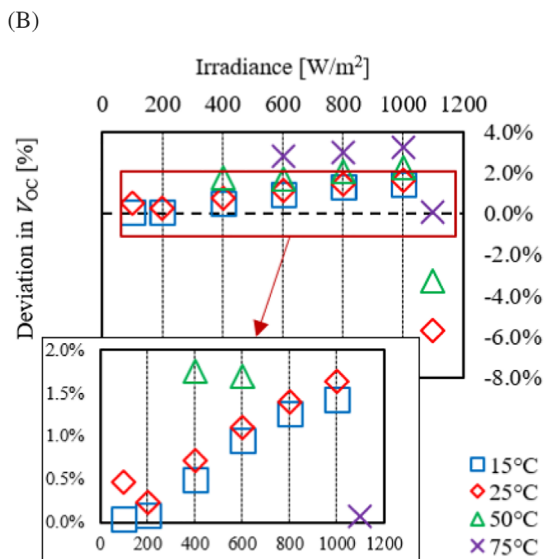
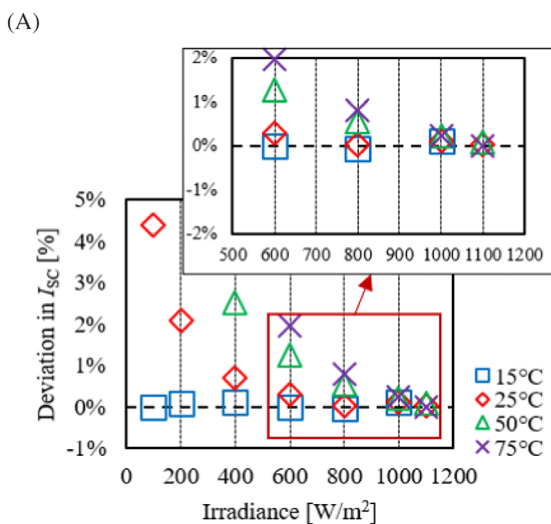


FIGURE 13 The deviation in (A) I_{SC} , (B) V_{OC} and (C) P_{MAX} of translated I - V curves to each conditions utilizing the 3-curve CP3 for HJT-2. The I - V curves selected to translate are the I - V curves measured at 100 W/m^2 , 15°C; 1100 W/m^2 , 75°C and 800 W/m^2 , 25°C (see Table 3 [3C-CP3]).

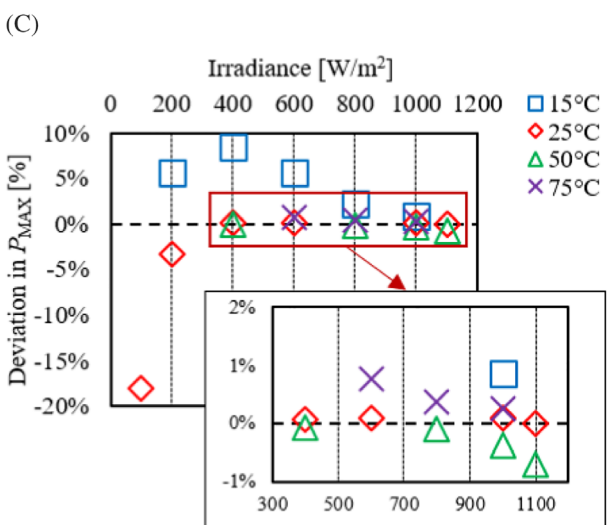
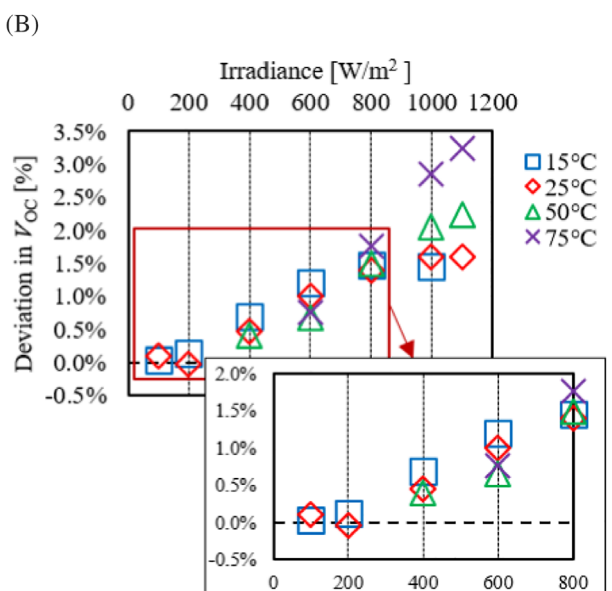
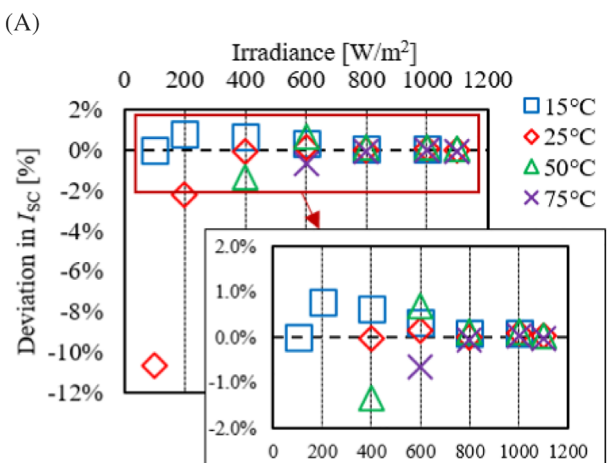
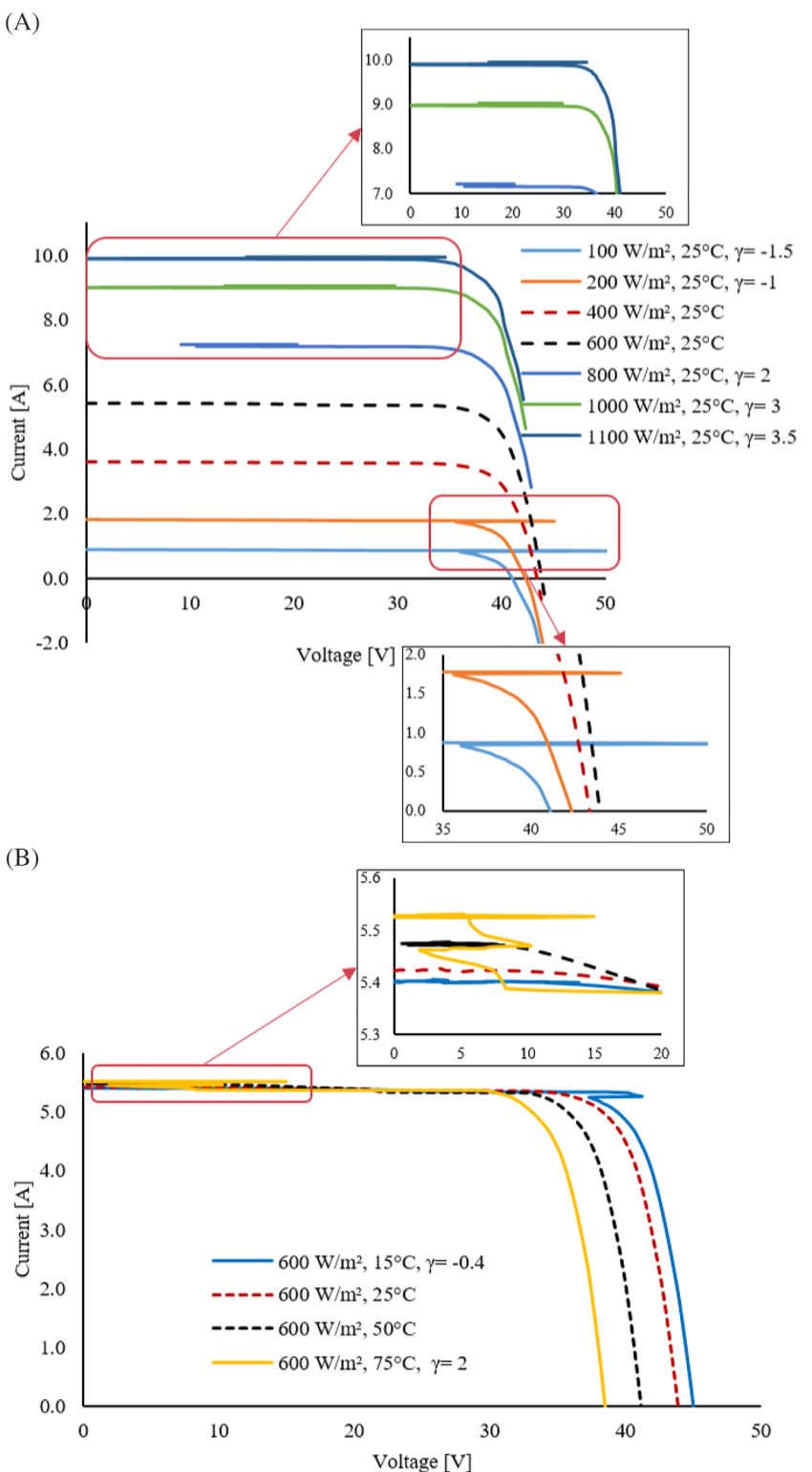


FIGURE 14 The deviation in (A) I_{SC} , (B) V_{OC} and (C) P_{MAX} of translated I - V curves to each conditions utilizing the 4-curve CP3 for HJT-2. The I - V curves selected to translate are the I - V curves measured at 100 W/m^2 , 15°C; 1100 W/m^2 , 75°C; 600 W/m^2 , 50°C and 800 W/m^2 , 25°C (see Table 3 [4C-CP3]).

FIGURE 15 (A) I-V curves of module HJT-2 translated to different irradiances, at 25°C by CP3. The dashed curves are measured at 400 W/m², 25°C and 600 W/m², 25°C; (B) I-V curves of module HJT-2 translated to different temperatures, at 600 W/m² by CP3. The dashed curves are measured at 600 W/m², 25°C and 600 W/m², 50°C.



value used by CP4*. It also indicates a distinct improvement in V_{OC} calculation for HJT-2 and LSH-1. CP4* produces a comparable V_{OC} in the other DUTs. The results demonstrated that a more accurate determination of R_S would effectively improve the accuracy of P_{MAX} of CP4. However, the method utilized by CP4 to determine R_S is the only one that can be used when only one I-V curve is available. The results also demonstrate that CP4 provides accurate results which are

comparable with CP1 and CP2 at test conditions within $\pm 40\%$ of irradiance and $\pm 25^\circ\text{C}$ of the target reporting test conditions.

Similarly to CP1, the high RMSE value in the case of LSH-1 is attributed to the shift of I-V curve caused by the temperature correction. The temperature correction leads to an I-V curve shift on the voltage axis (see Equations 22 and 23), which results in an inaccurate I_{SC} in the case of low shunt-resistance DUT (LSH-1).

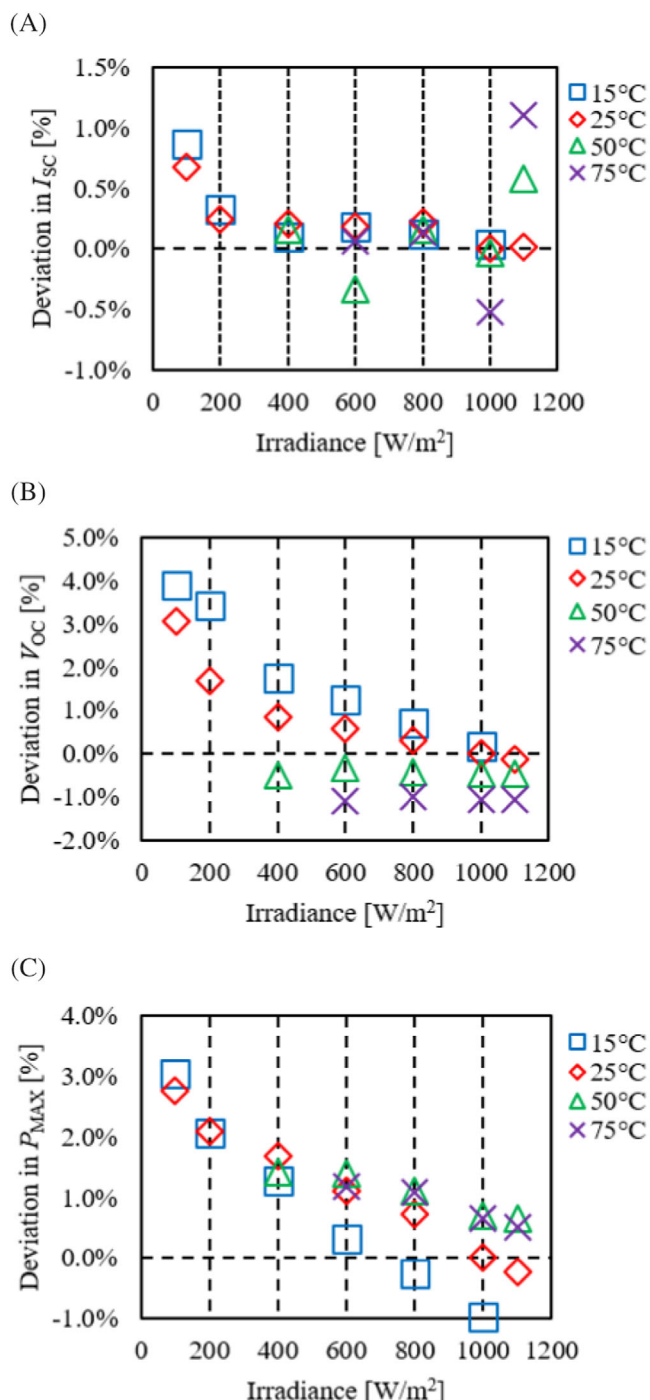


FIGURE 16 The deviation in (A) I_{SC} , (B) V_{OC} and (C) P_{MAX} of translated I - V curves to STC utilizing the CP4 for HJT-2. The shown DUT exhibited worst-case deviations for CP4.

4 | CONCLUSION

In this work, we evaluated the four I - V curve correction procedures that are listed in IEC 60891:2021.³ MBE and RMSE are employed to evaluate the performance of all CPs in terms of three electrical

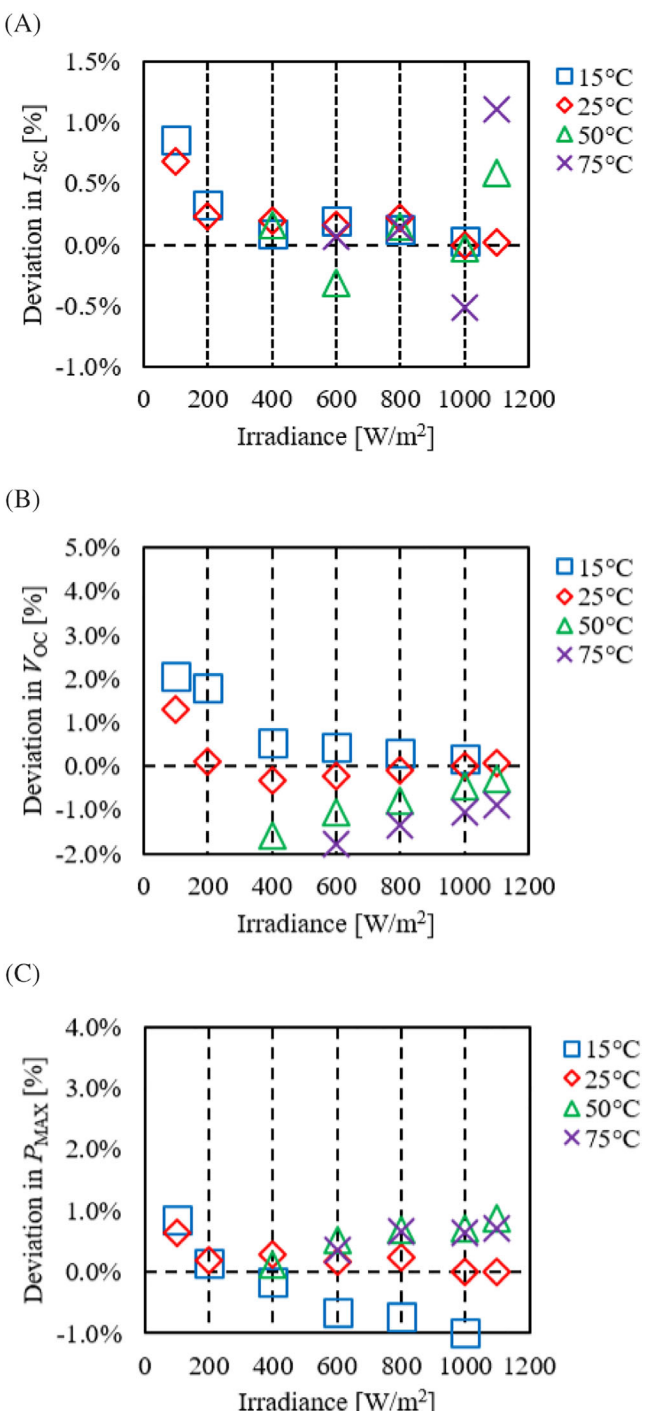


FIGURE 17 The deviation in (A) I_{SC} , (B) V_{OC} and (C) P_{MAX} of translated I - V curves to STC utilizing the CP4* for HJT-2.

parameters. The acceptable threshold value of both indexes are set to $\pm 1\%$ in this work.

CP1 generally performs accurate I - V curve correction. The MBE and RMSE for all six DUTs in all three electrical parameters are within $\pm 1\%$ (see Table 4). In the detailed analysis, it was also noticed that I - V

curves have to be measured adequately far enough into the negative current regime to achieve complete *I-V* curves after translation from low irradiance to high irradiance when employing CP1.

CP2 produces accurate results for most DUTs, but gives catastrophic results for the low shunt-resistance test sample LSH-1. We showed that it is not recommended to use CP2 for *I-V* translation over irradiances beyond the general constraints for *I-V* curve measurements set by IEC 60904-1, if the DUT has low shunt-resistance and large current leakage. To improve this, a new CP named “low-shunt CP2” was developed and presented in this paper (see Section 2.3.3). As shown by a comparison of Figures 10 and 12 and by the data summarized in Table 4 as well as in the supporting information (Tables S30 and S31), the low-shunt CP2 improves the performance of the correction for low shunt-resistance modules; noticeably the MBE value for P_{MAX} improves from -10.26% to -1.32% (see Table 4), and the RMSE value for P_{MAX} improves from 19.52% to 1.77% . For all DUTs with no issues of current leakage and of low shunt-resistance, low-shunt CP2 produced results comparable to those achieved by CP2. Therefore, low-shunt CP2 could be used universally.

Both CP3 methods provide good agreement in V_{OC} with RMSE and MBE values for V_{OC} within $\pm 0.65\%$ (Table 4), except for HJT-2. The I_{SC} and P_{MAX} deviations are unexpected, with both CP3 methods producing over 1.3% in I_{SC} and over 1.65% in P_{MAX} in terms of RMSE. The results demonstrated that CP3 works well over a broad range of irradiances and temperatures, as long as interpolation is used. However, when extrapolation is carried out, a variable significant distortion of the corrected *I-V* curves may occur in the I_{SC} or P_{MAX} region. The severity of the distortion depends on the value of the interpolation constant γ (see Section 2.3.4). A large negative/positive γ value (outside the range from 0 to 1) could aggravate distortion. Therefore, it is recommended to prefer interpolation and employ extrapolation with caution.

CP4 generally produces accurate calculation for I_{SC} and V_{OC} . The MBE and RMSE (Table 4) of all DUTs for all I_{SC} of CP4 are within $\pm 0.72\%$, except for LSH-1. The MBE and RMSE in V_{OC} calculated by CP4 are within $\pm 1.05\%$ for most DUTs, except for HJT-2. The MBE and RMSE in P_{MAX} are over 1% for most DUTs, except for PERC-1 and H-1. We verified then how a different method for the determination of R_S affects the correction accuracy of CP4, we labelled this by CP4*. In relation to this, the MBE and RMSE in P_{MAX} were significantly improved when the CP1 R_S determination method was applied instead of the R_S determination from the single *I-V* curve (see Table 4). It has to be mentioned, though, that the original CP4 R_S determination is the only method that works when only a single *I-V* curve is available, which might represent a good compromise between accuracy and data availability in the frame of particular applications or test conditions.

In view of these results, generally all four *I-V* correction procedures produce accurate results over a broad range of irradiances and temperatures, but the user should be well aware of the benefits and drawbacks of each CP. The selection of the CP to use in a particular

case will first and foremost depend on what experimental data is available or can be obtained.

If all the relevant correction parameters can be obtained from the measured *I-V* curves, either CP1 or CP2 should be used. Their accuracy is highly comparable, with two exceptions. First, if the *I-V* curve has not been measured down to a sufficiently negative current level (see Figure 8), CP2 is to be preferred because it inherently does not need this type of data. CP1 on the contrary relies on it and will produce erroneous results in its absence. Second, if the DUT has a low shunt-resistance, CP1 and CP2 are both not recommended, because CP1 does result in inaccurate I_{SC} for the temperature correction process and CP2 does result in significant deviations in this case due to an enhanced steep slope of the *I-V* curve near I_{SC} (see Figure 11). The problem with CP2 can be mostly overcome by using the low-shunt CP2, which has been proposed and detailed in this paper. However, at present the use of the low-shunt CP2 would not comply with the requirements to perform *I-V* curve corrections according to IEC 60891, because at present the low-shunt CP2 is not included in this IEC standard.

If only a few (three or four) measured *I-V* curves are available, CP3 is the method of choice for linear PV devices. This limited number of *I-V* curves is usually insufficient to determine the correction coefficients required for CP1 and CP2 within an acceptable uncertainty. When the translation with CP3 is carried out by linear interpolation, satisfactory results are obtained. It is therefore suggested to measure the *I-V* curves at higher and lower irradiances compared with the target irradiance if the latter is not directly achievable. When extrapolation is required, more caution needs to be exercised as artefacts and distortions can appear in the corrected *I-V* curve.

Finally, if only one single measured *I-V* curve is available and the correction parameters for CP1 and CP2 cannot be known in any way, CP4 is the only CP that can be used. Considering the limited amount of information available, the results are satisfactory. The accuracy of CP4 can be improved by using the R_S value as determined in CP1, but this would require more experimental data to be available. Similarly to CP1, CP4 becomes inaccurate, mainly for V_{OC} , in the case of insufficient data in the negative-current portion of the *I-V* curve. The only method capable of addressing this case, which is quite common, is CP2. The other three CPs should be preferably used only if sufficient experimental data into the negative current regime has been measured.

ACKNOWLEDGEMENTS

The work presented has been partially made under 19ENG01 Metro-PV. This project 19ENG01 Metro-PV has received funding from the EMPIR programme, co-financed by the Participating States and from the European Union's Horizon 2020 research and innovation programme.

DATA AVAILABILITY STATEMENT

Research data are not shared.

ORCIDChristos Monokroussos  <https://orcid.org/0000-0002-6953-0638>**REFERENCES**

1. IEC 60904-3. 2019. Photovoltaic Devices - Part 3: Measurement Principles for Terrestrial Photovoltaic (PV) Solar Devices with Reference Spectral Irradiance Data.
2. IEC TS 61836. 2016. Solar Photovoltaic Energy Systems - Terms, Definitions and Symbols.
3. IEC 60891. 2021. Procedures for Temperature and Irradiance Corrections to Measured I-V Characteristics.
4. Sandstrom JD. *A Method for Predicting Solar Cell Current- Voltage Curve Characteristics as a Function of Incident Solar Intensity and Cell Temperature*. National Aeronautics and Space Administration (NASA); 1967.
5. IEC 60891. 2009. Photovoltaic Devices - Procedures for Temperature and Irradiance Corrections to Measured I-V Characteristics.
6. Hishikawa Y, Tsuno Y, Kurokawa K. Translation of the I-V Curves of Various Solar Cells by Improved Linear Interpolation. In: 21st European Photovoltaic Solar Energy Conference (EUPVSEC); 2006.
7. Hishikawa Y, Takenouchi T, Higa M, Yamagoe K, Ohshima H, Yoshita M. Translation of solar cell performance for irradiance and temperature from a single I-V curve without advance information of translation parameters. *IEEE J Photovolt*. 2019;9(5):1195-1201. doi: [10.1109/jphotov.2019.2924388](https://doi.org/10.1109/jphotov.2019.2924388)
8. Herrmann W. Zur Leistungsbemessung von Photovoltaik-Modulen Mit Sonnensimulationsanlagen. 2001.
9. Bishop JW. Computer simulation of the effects of electrical mismatches in photovoltaic cell interconnection circuits. *Solar Cells*. 1988;25(1):73-89. doi: [10.1016/0379-6787\(88\)90059-2](https://doi.org/10.1016/0379-6787(88)90059-2)
10. Monokroussos C, Etienne D, Morita K, Dreier C, Therhaag U, Herrmann W. Accurate power measurements of high capacitance PV modules with short pulse simulators in a single pulse. In: 27th European Photovoltaic Solar Energy Conference (EUPVSEC); 2012.
11. IEC 61853-1. 2011. Photovoltaic (PV) Module Performance Testing and Energy Rating—Part 1: Irradiance and Temperature Performance.
12. Chai T, Draxler RR. Root mean square error (RMSE) or mean absolute error (MAE)? *Geosci Model Dev Discussions*. 2014;7(1):1525-1534. doi: [10.5194/gmdd-7-1525-2014](https://doi.org/10.5194/gmdd-7-1525-2014)

SUPPORTING INFORMATION

Additional supporting information can be found online in the Supporting Information section at the end of this article.

How to cite this article: Xu W, Monokroussos C, Müllejans H, Herrmann W. Performance evaluation of procedures used to correct measured I-V characteristics of photovoltaic modules for temperature and irradiance. *Prog Photovolt Res Appl*. 2023; 31(10):981-998. doi: [10.1002/pip.3702](https://doi.org/10.1002/pip.3702)